

Received March 20, 2020; reviewed; accepted July 13, 2020

Experimental research on energy-size distribution model of coal particle bed comminution

Qiang Zhou ¹, Qing Guo ¹, Yongtai Pan ¹, Changyong Zhu ², Yinghua Wei ²

¹ China University of Mining and Technology Beijing, School of Chemical and Environmental Engineering, Beijing, 100083, China

² Shenhua Ningxia Coal Industry Group CO., LTD Taixi CPP, Ningxia Shi Zuishan 753000, China

Corresponding author: pan_yongtai@126.com (Yongtai Pan)

Abstract: In order to accurately predict the particle size distribution (PSD) of coal particle bed comminution under different applied pressures, the tests of two kinds of coal with four size fractions under five different applied pressures were carried out by TAW-3000 hydraulic servo testing machine. The Gaudin-Schumann(G-S) distribution is extended by the fractal theory and the JK size-dependent breakage model is discussed. Two mathematical models for predicting PSD of crushing products in coal particle bed comminution are proposed. Results show that the relationship between the mass-specific energy and applied pressure is linear. Because of the protective effect of fine particles, the change of particle size modulus d_0 in G-S distribution is not significant, while the distribution parameter a decreases logarithmically with the increase of mass-specific energy. With the decrease of size fraction, the crushability of coal particle bed decreases, and a master curve can be used to fit the comminution characteristics of coal particle bed with different size fractions. The extended G-S distribution model and the JK size-dependent breakage model have better fit the results of coal particle bed comminution. This research provides a useful reference for the mathematical modelling of coal particle bed comminution.

Keywords: coal, particle bed comminution, the extended G-S distribution, the JK size-dependent breakage model, mathematical modelling

1. Introduction

The coal comminution is one of the important operation units to realize the clean coal processing and utilization of coal. Improving the energy utilization efficiency of coal comminution and controlling the particle size distribution (PSD) have been the focus of research all around the world (Zuo et al., 2012). The comminution of coal is a very complex non-linear process which has the characteristics of high energy consumption, and low energy efficiency. Therefore, it is of great importance to study the fragmentation mechanism of coal and establish the relationship between energy input and PSD. For more than one hundred years, much attention has been given to the energy-size reduction relationships, in which laws of Rittinger (1867), Kick (1885) and Bond (1952) are notable (Liu et al., 2016). To describe the degree of breakage concerning particle size effect and specific energy input, a size-dependent breakage model was developed in 2006, and published in 2007 (Shi and Kojovic, 2007).

Many studies have investigated the principle of single particles and particle bed comminution. A large number of valuable results have been obtained, such as assessment of particle strength, estimation of energy requirement for size reduction and PSD, and equipment modelling (Shi, 2016; Tavares and King, 1998; Jiang et al., 2018; Schönert, 1996). The mechanism of particle material comminution has been revealed, which provides a theoretical basis for improving and optimizing the existing comminution equipment and developing energy-saving, environmental comminution equipment. As a result of impact experiments, a variety of correlations to define the breakage function have been developed. It

should be noted that some researchers correlate breakage function with the impact velocity (Duo et al., 1996; Kalman et al., 2004; Petukhov and Kalman, 2003; Salman et al., 2002), while others with the kinetic impact energy (Austin, 2002; Peukert, 2004). The standard PSD equations are Gaudin-Schumann (G-S) distribution, Rosin-Rammler (R-R) distribution, lognormal distribution and truncated lognormal distribution (Meier et al., 2009). The PSD models are the summary of experience, but the parameters in most PSD models lack specific physical significance. Turcotte (1986) used the fractal method to describe the PSD quantitatively and linked it with a specific comminution model, which was of considerable significance to the study of the comminution process. Gong (2018) systematically studied the comminution characteristics of copper and gold ore under slow compression, impact and particle bed comminution. The sieving data under different comminution methods were fitted well with G-S distribution and R-R distribution. It was found that the particle size modulus (maximum particle size) of G-S distribution did not change significantly in the process of particle bed comminution, which confirmed the protective effect of fine particles in particle bed comminution. Xu (2018) established a quantitative relationship between the PSD parameters and the input energy in the G-S model by using the fractal theory. The comminution index t_{10} is used as a "bridge" to establish a quantitative relationship between breakage degree and comminution energy. It can also be used to predict the particle size distribution of ore comminution through the established family of t -curves. Therefore, the interest in the improvement of comminution and its fundamental aspects remains undiminished. The comminution efficiency improvement should be directed not only towards the machine development that enhances energy utilization but also towards the design of grinding operations that make optimal use of existing machines.

In this paper, an energy-size distribution based on the extended G-S distribution is established, and the JK size-dependent breakage model incorporating particle size material characteristics and input energy is recommended. This research can provide a convenient method for the estimation PSD under different input energy in coal particle bed comminution.

2. Theory

2.1. The extended G-S distribution

Turcotte (1986) proposed a fractal model for the particle fragmentation based on the notion of a scale-invariant cascade of fragmentation. In this model, a parent particle is composed of a population of structural units of fixed size d_0 . A fraction P of this mass fragments into smaller units of size $d_1=rd_0$, where r is reduction ratio (is a constant <1). A fraction P of this mass in turn fragments into units of size $d_2=rd_1$. The division process is repeated across a range of cascade of scales, resulting in a geometric progression of fragment sizes. If M_i is the cumulative mass of fragments $\leq d_i$, then the model may be written simply as $M_{i+1}=PM_i=P^iM_T$. A power-law relation yields in terms fragment size d_i as follows.

$$\frac{M(\leq d_i)}{M_T} = \left(\frac{d_i}{d_0}\right)^\alpha \quad (1)$$

where $\alpha=3-D$, D is the fragmentation fractal dimension. The fragmentation fractal dimension is related to the probability of fracture in the form of

$$D = 3 - \frac{\log P}{\log r} \quad (2)$$

where P is the probability of fracture. Vogel et al. (2003) obtained the breakage probability of particles that are broken as a function of fracture energy fundamentally. The breakage probabilities of brittle particles are described with Weibull statistics. Weibull's brittle fracture equation is given by (Xu et al., 2018)

$$P = \left(\frac{\sigma}{\sigma_0}\right)^m \quad (3)$$

where σ is the value of σ_0 such that 37% of the total number of test particles survival, P is the probability of failure (defined as the cumulative relative frequency distribution for σ), and m is a constant corresponding to the moments of the Weibull distribution, called the Weibull modulus. Substituting Eq. (3) into Eq. (2), the relationship between the fragmentation fractal dimension and the applied stress is given by

$$D = a + b \log \sigma \quad (4)$$

where $a = 3 + m \log \sigma_0 / \log r$, $b = -m / \log r$. The mass-specific energy is given by (Tavares, 1998)

$$E_m = C \sigma^{\frac{5}{3}} \quad (5)$$

Combining Eq. (4) and Eq. (5) yields the relation of the fragmentation fractal dimension to the specific fracture energy as follows:

$$D = A + B \log E_m \quad (6)$$

where $A = 3 + m \log \sigma_0 / \log r + 3m \log C / (5 \log r)$, $B = -3m / (5 \log r)$.

$$\alpha = 3 - D = P + Q \log E_m \quad (7)$$

where $P = 3 - A$, $Q = -B$.

The extended G-S distribution is given by

$$y = 100 \times \left(\frac{d_i}{d_0} \right)^{(P + Q \log E_m)} \quad (8)$$

2.2. The prior art JK model and the JK size-dependent breakage model

The prior art JK model describes the relationship between t_{10} and E_m , as follows:

$$t_{10} = A(1 - e^{-bE_m}) \quad (9)$$

where t_{10} is a size distribution 'fineness' index defined as the progeny percent passing one-tenth of the initial mean particle size (%), E_m is the mass-specific energy (kWh t^{-1}), and A and b are the ore impact breakage parameters determined by the drop weight test (Napier-Munn et al., 1997)

Based on dimensional analysis and mechanical considerations, Vogel and Peukert (2003) quantified the description of the breakage probability and breakage function, as follows:

$$S = 1 - \exp[-f_{mat} \cdot x \cdot k \cdot (W_{m,kin} - W_{m,min})] \quad (10)$$

where S is the breakage probability, f_{mat} is the material breakage property ($\text{kg J}^{-1} \text{m}^{-1}$), x is the initial particle size (m), $W_{m,kin}$ is the mass-specific kinetic impact energy (J kg^{-1}), $W_{m,min}$ is the threshold energy below which breakage does not occur (J kg^{-1}), and k is the successive number of impacts with the single impact energy.

Shi and Kojovic (2007) modified Vogel and Peukert's breakage probability model to describe the breakage index t_{10} (%) with material property, particle size and net cumulative impact energy, as follows:

$$t_{10} = M \{1 - \exp[-f_{mat} \cdot x \cdot k \cdot (W_{m,kin} - W_{m,min})]\} \quad (11)$$

where M represents the maximum t_{10} for material subject to breakage (%), and E_{min} the threshold energy (J kg^{-1}) (the units of the other variables are the same as in Eq. (10)).

Nadolski et al. (2014) presented a revised version of Eq. (11), in which E_{min} was set to zero, and particle size x replaced with the square root of x . Eq. (12) can well represent the particle size effect and give a better fit in multilayer particle compression tests.

$$t_{10} = M[1 - \exp(-f_{mat} \cdot x^{0.5} \cdot k \cdot E_m)] \quad (12)$$

Nadolski (2015) further modified Eq. (12) by changing the exponent 0.5 to more flexible exponent n (Eq. (13)):

$$t_{10} = M[1 - \exp(-f_{mat} \cdot x^n \cdot k \cdot E_m)] \quad (13)$$

3. Materials and method

3.1. Materials

The bituminous coal from Zhun Geer of Inner Mongolia and the anthracite from Tai xi of Ningxia were used for carrying out the particle bed comminution. Two of the tested materials are illustrated in Fig. 1. As shown in Fig. 1(b), the structure of the anthracite is compact with few apparent cracks. The properties of the coal are shown in Table 1.

The raw coals were crushed by jaw crusher. The crushed sample was sieved to produce a sufficient stock of several size fractions, namely 13-6, 6-3, 3-1, and 1-0.5 mm. The sieved particles were mixed evenly. A sample weight of 60 g was comminuted under a set of bed pressures. Three parallel tests were required under the same test conditions.

Table 1. Properties of the coal

Coal type	Compressive strength (MPa)	Tensile strength (MPa)	Elasticity modulus (GPa)	Poisson's ratio	Density (g·cm ⁻³)	HGI
Bituminous coal	19.93	1.73	3.80	0.31	1.46	61
Anthracite	20.89	3.00	4.92	0.27	1.52	44

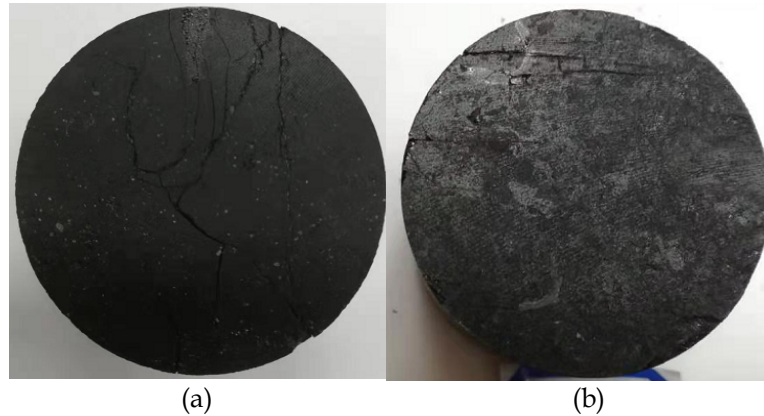


Fig. 1. Coal samples for the tensile tests. (a) Bituminous coal. (b) Anthracite

3.2. Apparatus and experimental methods

The TAW-3000 hydraulic servo test system, shown in Fig. 2, was used for carrying out particle bed comminution. Comminution tests were carried out in a piston-die assembly loaded. The piston with a diameter of 50 mm was snugly fitted into die, 50.2 mm diameter, to make a fully confined coal particle bed. The mass of solids forming the particle bed was 60 g in all tests. The particle beds compressed at a slow rate of loading (5 mm min^{-1}) up to the desired maximum force levels of 10, 20, 30, 40, and 50 kN, corresponding to the approximate bed pressure of 5.09, 10.19, 15.27, 20.38, and 25.48 MPa, respectively. Force-displacement data were logged digitally and integrated numerically up to the maximum displacement to obtain the total work of compression. A series of standard sieves with specifications from 0.074 mm to 13 mm were selected to screen 120 comminution products with four size fractions under different loading intensities. The EW-300A (accuracy is $\pm 0.0001 \text{ g}$) electronic balance was used to weigh the sieving products of each size fraction, and the relative weight loss value of the size fraction is less than 0.5%. After weighing, the sieving products of each size fraction were poured into the sample bag, respectively and store them for later use.

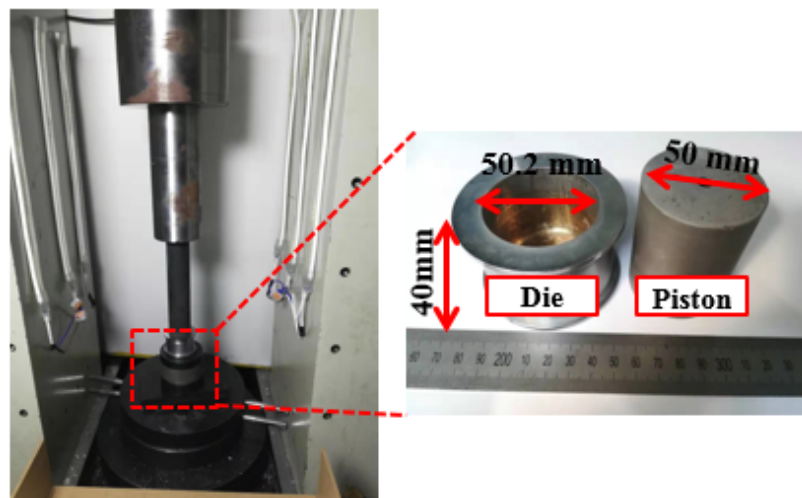


Fig. 2. TAW-3000 hydraulic servo test system

4. Results and discussion

4.1. Force-displacement curves and energy absorption

Fig. 3 shows the force-displacement curves of the bituminous coal sample with 3-1 mm size fraction. The displacement curve is divided into four stages including compaction stage (OA), damage stage (AB), fragmentation stage (BC), and welding stage (CD). The piston moves rapidly with lower forces in the compaction stage where the particles are rearranged. With increasing force and compaction, particles are stressed in quasi-triaxial or quasi-uniaxial model which may eventually lead to breakage and concomitant rearrangement, namely damage stage and fragmentation stage. The force-displacement curves become steeper with increasing compaction and show a regular trend with the size fraction, namely welding stage.

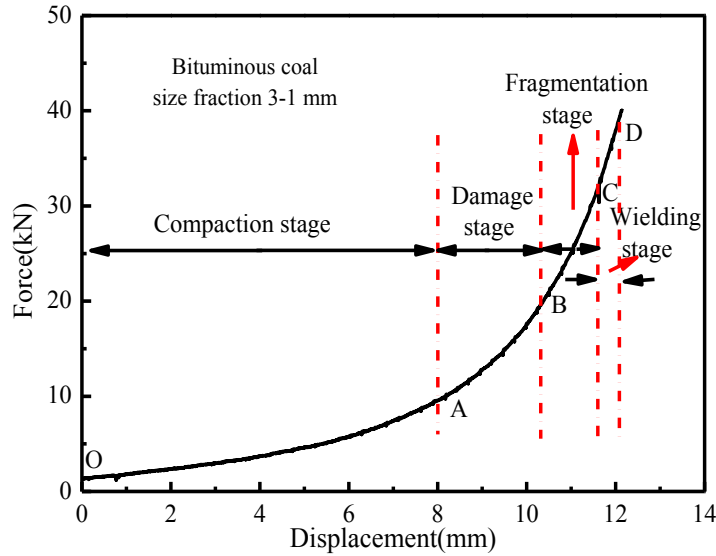


Fig. 3. Force-displacement curves of bituminous coal size fraction 3-1 mm

As expected, the specific energy consumed for breaking the various size fractions increased as the applied load increased. The trend of the specific energy consumed as a function of the applied load increases as shown in Fig. 4. There is almost a linear increase in the specific energy absorbed with the increasing applied pressure within its experimentally studied range. There is no noticeable difference among coal particle beds of the bituminous coal with four size fractions. However, for particle beds of the anthracite with four size fractions, a smaller size fraction absorbs more energy at the same applied stress. A probable explanation for this behaviour is the result of the microstructure of the material (Liu et al., 2012; Abouzeid et al., 2018).

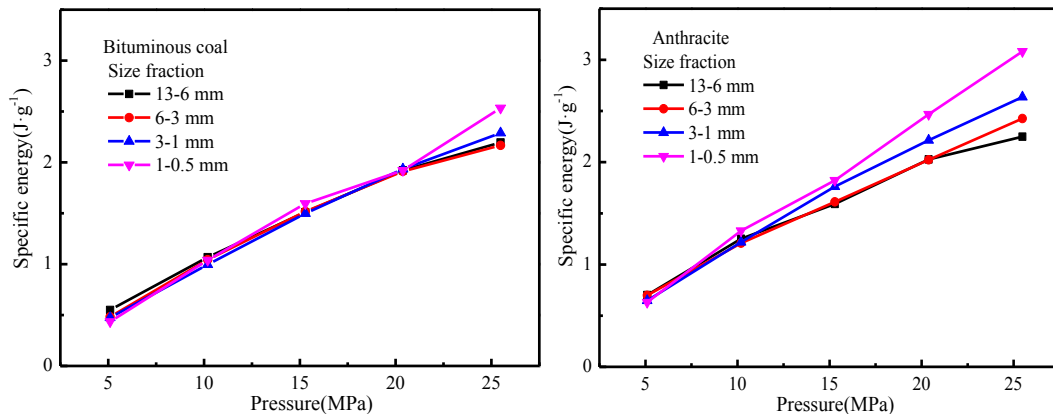


Fig. 4. Specific energy absorption at different levels of applied pressure in particle bed comminution of bituminous coal and anthracite

4.2. G-S distribution and its extension

The PSDs of the progeny fragments resulting from particle bed comminution tests were measured by the sieving and then fitted with the Eq. (1). The average coefficient of determination (R^2) is 0.96. The size fraction of 1-0.5 mm is taken as an example, as shown in Fig. 5.

As shown in Fig. 5, the product PSDs of the bituminous coal and anthracite samples comminuted in piston-die press shift progressively to fine size distributions as the applied pressure or equivalently the energy input increased. The shift in the size distribution curves is extra pronounced at low pressures. Fig. 5 suggests that the size distribution of bituminous coal is expectedly finer than anthracite. An explanation for this behaviour is that the HGI of anthracite is lower than bituminous coal, shown in Table 1.

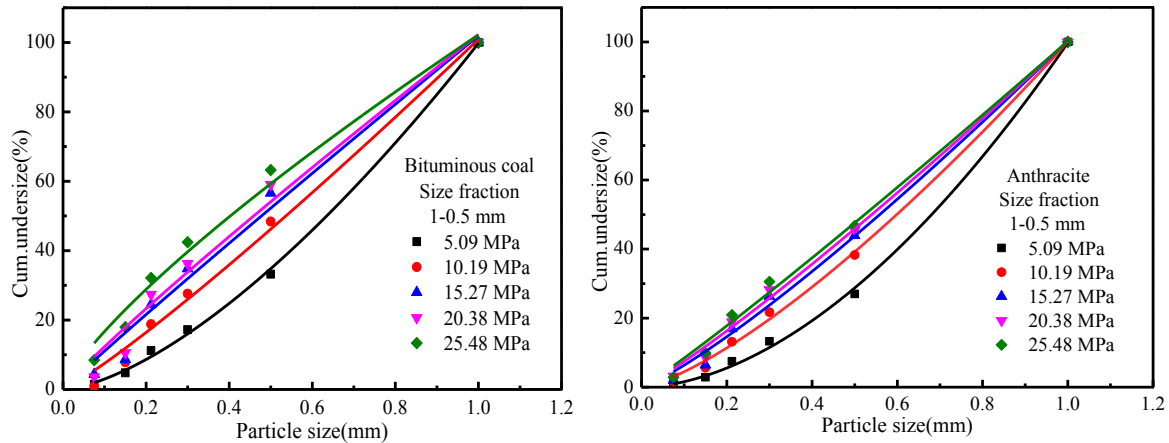


Fig. 5. Product size distributions of bituminous coal and anthracite in piston die-press at size fraction 1-0.5 mm and Eq. (1) fitting

As shown in Fig. 6, the particle size modulus d_0 in the G-S distribution did not vary with the increasing applied pressure. Because the fine particles sandwiched between two coarse particles are easy to be broken, the coarse particles wrapped by many fine particles are protected. Distribution parameter a in the G-S distribution decreases with the input energy. The a depends on the particle size, input energy and material property. The a of the bituminous coal and anthracite samples were collected and related to the input energy respectively as shown in Fig. 7. The relation between the a and the input energy is a logarithmic function, which can be described by Eq. (7). The parameters of P and Q of the bituminous coal and anthracite are listed in Table 2.

Previous work has found that the crack density of large particles is much greater than for smaller particles (Krajcinovic, 1996; Tavares and King, 1998). Because of this, bigger particles tend to be weaker

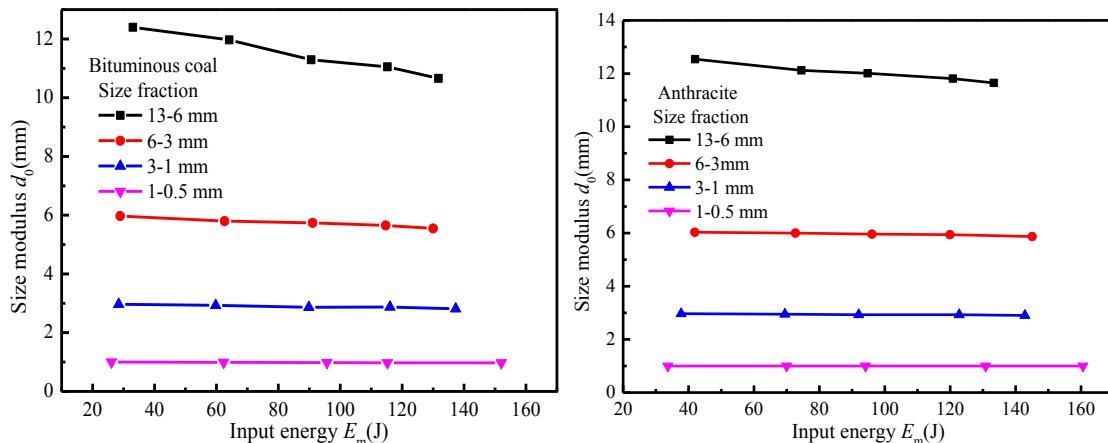


Fig. 6. Size modulus d_0 at different levels of applied pressure in particle bed comminution of bituminous coal and anthracite

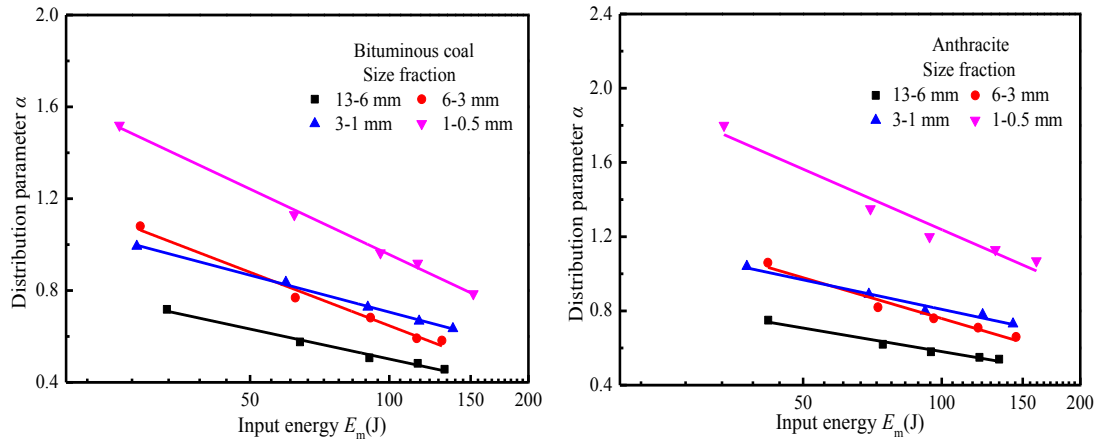


Fig. 7. Distribution parameter α at different levels of applied pressure in particle bed comminution of bituminous coal and anthracite

Table 2. Parameters of P and Q

Type	Size fraction(mm)	P	Q	R^2
Bituminous coal	13-6	1.37	-0.43	0.986
	6-3	2.19	-0.77	0.983
	3-1	1.77	-0.53	0.997
	1-0.5	2.85	-0.94	0.995
Anthracite	13-6	1.42	-0.42	0.973
	6-3	2.22	-0.73	0.961
	3-1	1.86	-0.53	0.974
	1-0.5	3.40	-1.08	0.948

and easier to be broken than smaller particles. Therefore, a model for particle bed comminution incorporating particle size effect was verified, as follows:

$$\alpha = (P + Q \log E_m) \bar{x}^{-c} \tag{14}$$

where c is the model parameter, \bar{x} is the geometry average of size fraction.

The parameters of the model are obtained by the method of surface fitting, as shown in Fig. 8. The parameters of P , Q and c of bituminous coal and anthracite are listed in Table 3.

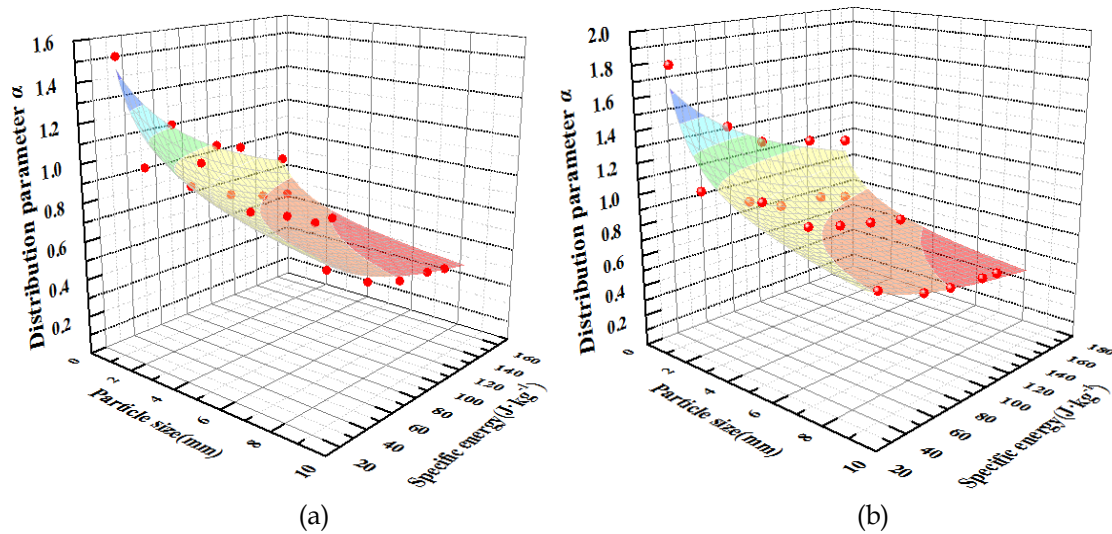


Fig. 8. The surface fitting of bituminous coal (a) and anthracite (b)

Table 3. Parameters of P , Q and c

Type	P	Q	c	R^2
Bituminous coal	2.51	-0.82	0.24	0.935
Anthracite	2.85	-0.88	0.29	0.911

Combining Eq. (14) and Eq. (1), as follow

$$y = 100 \times \left(\frac{d_i}{d_0}\right)^{(P+Q \log E_m) \bar{x}^{-c}} \quad (15)$$

According to Eq. (15), the distribution of particle products under different input energy can be predicted for a given material size fraction. The size fraction 13~6 mm of the anthracite is taken as an example. As shown in Fig. 9, comparison between measured (symbols) and fitted (lines) size distributions from Eq. (15), the average coefficient of determination, R^2 is 0.93.

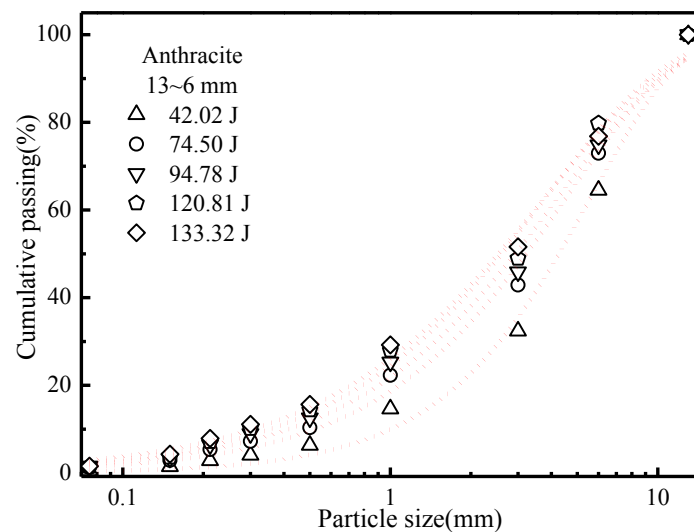


Fig. 9. Comparison between measured (symbols) and fitted (lines) size distributions from Eq. (15)

4.3. Family of t_n -curves of the bituminous coal and anthracite

The t_{10} index can be converted into a full PSD curve using a graph known as the family of t_n -curves which was first published by Narayanan (1985). Several researchers have confirmed that the mathematical relationships defined by the t_n -curves (Shi et al., 2007; Nadolski et al., 2014). The family of curves is universal for rock materials at different energy levels as shown in Eq. (16) to Eq. (20) (Gong et al., 2018). In this paper, this method is used to describe the coal particle bed comminution under different energy levels.

$$t_2 = \frac{a_2 \times t_{10}}{b_2 + t_{10}} \quad (16)$$

$$t_4 = \frac{a_4 \times t_{10}}{b_4 + t_{10}} \quad (17)$$

$$t_{25} = a_{25} \times t_{10} \quad (18)$$

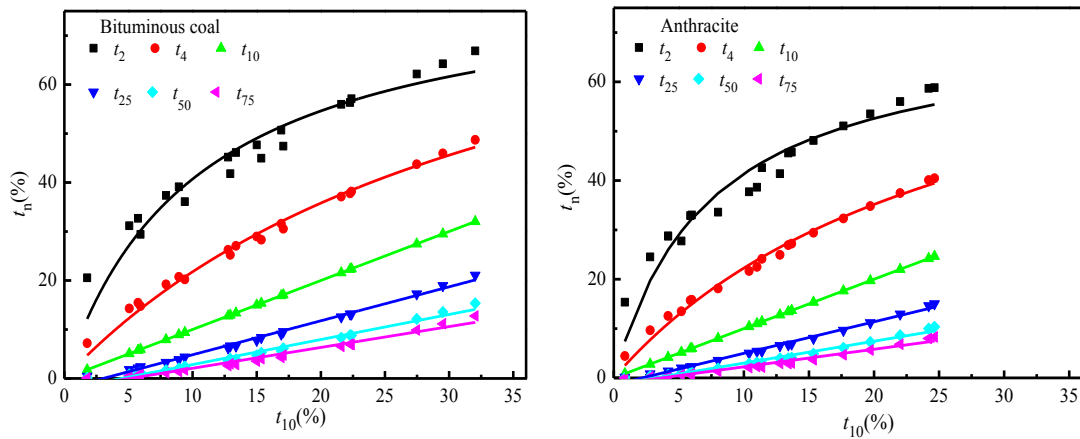
$$t_{50} = a_{50} \times t_{10} \quad (19)$$

$$t_{75} = a_{75} \times t_{10} \quad (20)$$

The values of t_2 , t_4 , t_{10} , t_{25} , t_{50} and t_{75} can be determined by sieving. The t_n is called the t_n index that the cumulative weight percentage passing through the $1/n^{\text{th}}$ screen. The value of a_2 , a_4 , a_{25} , a_{50} , a_{75} , b_2 and b_4 are model parameters. Data analysis results are arranged as shown in Fig. 10.

Fig. 10 and Table 4 show that a high degree of fit was achieved using Eq. (16) to Eq. (20). The average value of R^2 is higher than 0.96. Comparing model parameters of the bituminous coal with the anthracite, it is found the bituminous coal is more comfortable to be broken than the anthracite. The reason is that the compressive and tensile strength of the bituminous coal is less than the anthracite.

The parameters of a_2 , a_4 , a_{25} , a_{50} , a_{75} , b_2 and b_4 of bituminous coal and anthracite are listed in Table 4.

Fig. 10. Breakage parameters: t_n versus t_{10} for bituminous coal and anthraciteTable 4. Parameters of a_2 , a_4 , a_{25} , a_{50} , a_{75} , b_2 and b_4

Type	Parameter	$t_2(\%)$	$t_4(\%)$	$t_{25}(\%)$	$t_{50}(\%)$	$t_{75}(\%)$
Bituminous coal	a_n	82.92	100.57	0.69	0.51	0.43
	b_n	10.37	36.18			
	R^2	0.929	0.989	0.992	0.978	0.967
Anthracite	a_n	72.08	83.45	0.64	0.44	0.36
	b_n	7.41	27.48			
	R^2	0.921	0.988	0.992	0.976	0.965

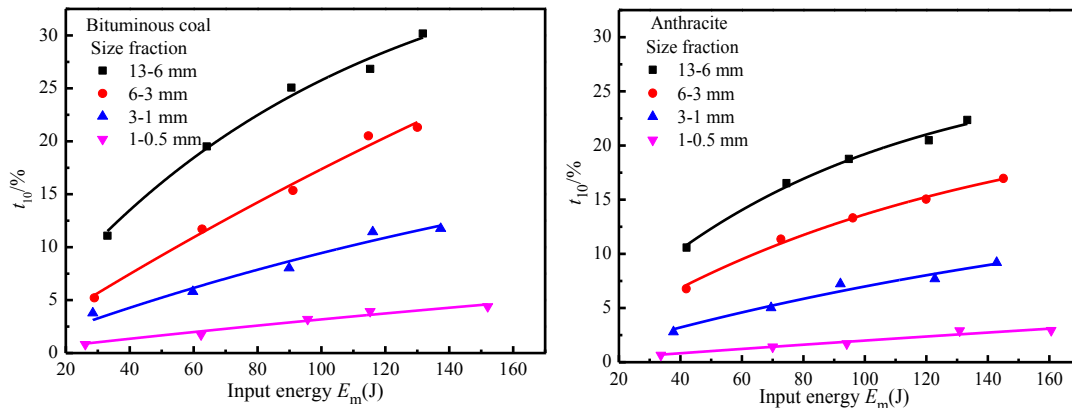


Fig. 11. The fitting results using the prior art JK model

4.4. The JK size-dependent breakage model of bituminous coal and anthracite

The t_n -curves are very useful, it can be used to transform or convert the t_{10} value into a full cumulative particle size distribution once the t_{10} is determined for the material. Firstly, the prior art JK model is used to fit the relationship between t_{10} and input energy, as shown in Fig. 11. With the increase of input energy, the t_{10} index of two kinds of coal with different size fraction increase. When the input energy is equal, the t_{10} index of coarse particles is bigger than small particles. The explanation for this behaviour is the result of the size effect of the particle. The product of A and b ($A \times b$) has been used as an indicator of ore hardness. As shown in Table 5, with the increase of size fraction, a product of A and b is much bigger.

The JK size-dependent breakage model takes a form similar to the JK prior art breakage model, but with particle size and breakage properties incorporated explicitly in the model. The Eq. (13) is used to fit the experimental data, shown in Fig. 12 and Table 6. For bituminous coal and anthracite, the model is fitted to the overall data using one set of model parameters.

Table 5. The prior art JK model parameters

Type	Size fraction(mm)	A (%)	b(J ⁻¹)	A × b(×10 ⁻² J ⁻¹)	R ²
Bituminous coal	13-6	40.38	0.010	0.404	0.988
	6-3	80.08	0.002	0.160	0.987
	3-1	26.81	0.004	0.107	0.977
	1-0.5	17.34	0.002	0.035	0.959
Anthracite	13-6	27.88	0.012	0.335	0.985
	6-3	24.09	0.008	0.193	0.993
	3-1	18.84	0.005	0.094	0.959
	1-0.5	18.17	0.001	0.018	0.940

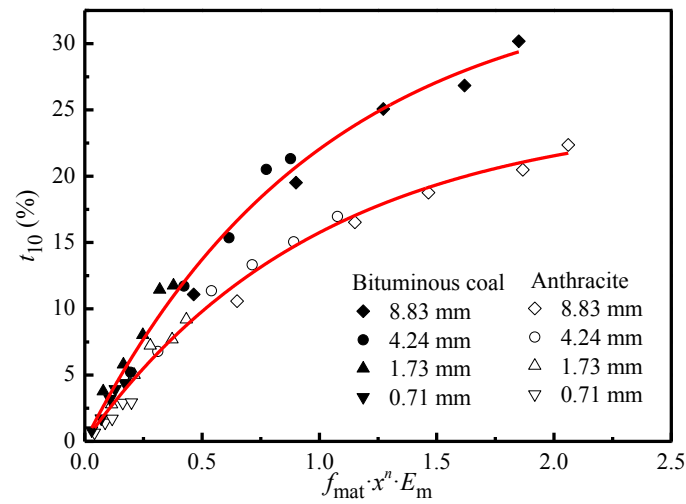


Fig. 12. The breakage model Eq. (13) fitted to measured points from the bituminous coal and anthracite particle bed comminution

Table 6. Fitted material constants for the Eq. (13)

Type	M (%)	f_{mat} (kg J ⁻¹ m ⁻ⁿ)	n	R ²
Bituminous coal	38.58	0.00157	0.91	0.988
Anthracite	24.93	0.00175	1.00	0.986

Two mathematical models proposed above can predict the PSD of different types of coal particles under different applied pressures. Although the accuracy of the extended G-S distribution model is slightly lower than that of the JK size-dependent breakage model, the PSD can be predicted by determining the three parameters (P , Q , and c) in the model. However, the JK size-dependent breakage model firstly determines the three parameters (M , f_{mat} , and n) in the model; secondly, the t_n - t_{10} curve cluster of the coal is established; finally, the PSD is obtained by spline interpolation. The JK size-dependent breakage model is more time-consuming and labour-intensive than the extended G-S distribution model to predict the PSD of different types of coal particles under different applied pressures. Since the coefficient of determination was reduced to a permissible degree, the extended G-S distribution model is deemed acceptable.

5. Conclusions

There is almost a linear increase in the specific energy absorbed with the increasing applied pressure within its experimentally studied range. There is no noticeable difference among coal particle beds of the bituminous coal with four size fractions. However, for particle beds of the anthracite with four size fractions, a smaller size fraction absorbs more energy at the same applied stress, a probable explanation for this behaviour is the result of the microstructure of the material.

The particle size modulus d_0 in the G-S distribution does not vary with the increasing applied pressure. The relation between the a and the input energy is a logarithmic function. The extended G-S distribution model can be used to predict PSD under coal particle bed comminution.

The prior art JK model and the JK size-dependent breakage model can also be used to access the coal particle bed comminution property and predict PSD under coal particle bed comminution.

Acknowledgements

The Fundamental Research Funds supported this work for the Central Universities (NO.2010YH11) and Shenhua Ningxia Coal Industry Group Co., Ltd. Tai xi Coal Preparation Plant, Shi Zuishan Ningxia 753000, China.

References

- ZUO, W.R., ZHAO, Y.M., DUAN, C.L., 2012. *Experiment study on impact crushing of coal based on S-Kojovic model*. Coal Science and Technology, 40(6), 117-120.
- LIU, X.M., ZHANG, M., HU, N., YANG, H.R., LU, J.F., 2016. *Calculation model of coal comminution energy consumption*. Minerals Engineering, 92, 21-27.
- SHI, F., KOJOVIC, T., 2007. *Validation of a model for impact breakage incorporating particle size effect*. International Journal of Mineral Processing, 82(3), 156-163.
- SCHÖNERT, K., 1996. *The influence of particle bed configurations and confinements on particle breakage*. International Journal of Mineral Processing, 44, 1-16.
- SHI, F., 2016. *A review of the applications of the JK size-dependent breakage model part 1: ore and coal breakage characterizations*. International Journal of Mineral Processing, 155, 118-129.
- JIANG, H., ZHOU, Y.D., CHI, C.J., 2018. *Transparent confined compression tests on particle beds: Observations and implications*. Powder Technology, 336, 339-349.
- TAVARES, L.M., KING, R.P., 1998. *Single-particle fracture under impact loading*. International Journal of Mineral Processing, 54(1), 1-28.
- DUO, W., BOEREFIJN, R., GHADIRI, M., 1996. *Impact attrition of fluid cracking catalyst*. Proceedings of the 5th International Conference on Multiphase Flow in Industrial Plants, Amalfi, Italy.
- KALMAN, H., HUBERT, M., GRANT, E., 2004. *Fatigue behavior of impact comminution and attrition units*. Powder Technology, 146, 1-9.
- PETUKHOV, Y., KALMAN, H., 2003. *A new apparatus for particle impact tests*. Particle & Particle Systems Characterization, 20, 267-275.
- SALMAN A.D., BIGGS C.A., FU J., 2002. *An experimental investigation of particle fragmentation using single particle impact studies*. Powder Technology, 128, 36-46.
- AUSTIN, L.G., 2002. *A treatment of impact breakage of particles*. Powder Technology, 126, 85-90.
- PEUKERT, W., 2004. *Material properties in fine grinding*. International Journal of Mineral Processing, 74, 3-17.
- MEIER, M., JOHN, E., WIECKHUSEN, D., 2009. *Generally applicable breakage functions derived from single particle comminution data*. Powder Technology, 194, 33-41.
- TURCOTTE, D.L., 1986. *Fractals and fragmentation*, J.Geophys.Res, 91, 1921-1926.
- GONG, D.Z., NADOLSKI, S., SUN, C.B., 2018. *The effect of strain rate on particle breakage characteristics*. Powder Technology, 339, 595-605.
- Xu, Y. F., 2018. *The fractal evolution of particle fragmentation under different fracture energy*. Powder Technology, 323, 337-345.
- NADOLSKI, S., KLEIN, B., KUMAR, A., 2014. *An energy benchmarking model for mineral comminution*. Miner. Engineering, 65, 178-186.
- NADOLSKI, S., KLEIN, B., GONG, D., 2015. *Development and application of an energy benchmarking model for mineral comminution*. The 6th International Conference on Semi-Autogenous and High-Pressure Grinding Technology, Vancouver, Canada.
- SHI, F., ZUO, W., 2014. *Coal breakage characterization - part 1: breakage testing with the JKFCB*. Fuel, 117, 1148-1155.
- LI, G.B., TANG, C.A., XU, X.H., 1991. *Fractal geometric description of G-S distribution of rock crushing particle size*. The Chinese Journal of Nonferrous Metals, 1(1), 31-33.

- XU, Y. F., SONG, D.Q., CHU, F.F., 2016. *Approach to the Weibull modulus based on fractal fragmentation of particles*. Powder Technology, 292, 99-107.
- MUNN, N., MORELL, S., MORRISON, R.D., 1997. *Mineral comminution circuits: Their Operation and Optimization*. Minerals Engineering, 10, 349-350.
- VOGEL, L., PEUKERT, W., 2003. *Breakage behavior of different materials-construction of master curve for the breakage probability*. Powder Technology, 129, 101-110.
- SHI, F., KOJOVIC, T, BRENNAN, M., 2015. *Modelling of vertical spindle mills. Part1: Sub-models for comminution and classification*. Fuel, 143, 595-601.
- Narayanan, S. S., 1985. *Development of a laboratory single particle technique and its application to ball mill scale-up*. PhD Thesis. Brisbane: University of Queensland.
- ABOUZEID, A.Z.M. A., SEIFELNASSR, A. A. S., ZAIN G., 2018. *Breakage behavior of quartz under compression in a piston die*. Mining Metallurgy & Exploration.
- LIU, J.Y., LUO, K.Y., ZHOU, B.Z., 2012. *Experimental study on comminution of iron ores by particle bed compressive stressing*. Mining & Metallurgy, 21(4), 1-6.